ENGINEERING JOURNAL

Article

Modeling and Simulation of UWB Wave Propagation for Early Detection of Breast Tumors in Cancer Dielectric Imaging Systems

Ikram E. Khuda[a,b,*]

Iqra University, Defence View, Shaheed-e-Millat Road (Ext.), Karachi, Pakistan
E-mail: [a]ikram@iqra.edu.pk (Corresponding author), [b]ikramekhuda@gmail.com

Abstract. In this paper, we have proposed an analytical body (breast-tissue) propagation model in terms of scattering parameters towards the design goal of a suitable ultra-wide band, (UWB) transceiver for early breast tumor detection. The scattering parameters are reflection (Γ) and transmission coefficients (T). We considered a heterogeneous breast model consisting of skin, adipose and glandular tissues as body (breast) channel and planar wave to propagate through it for UWB frequency range. A tumor layer was also considered as an inner layer to investigate tumorous tissue effects. Effective dielectric properties and scattering parameters (through reflected/ scattered or forward transmitted signals) for the whole breast were determined. Due to dispersive nature of heterogeneous breast, Γ and T vary with frequency; showing their decisive nature for a particular center frequency of the UWB transceiver systems. In case of 2.0 GHZ and 4.5 GHz center frequency UWB system, the back propagated (reflected/ scattered) signals showed approximately 45.45% and 63.3% respectively higher amplitude than forward propagated signals for the breast channel with tumor, indicating high value of dispersion present in human breast tissues.

Keywords: S-parameters, UWB, transceiver, reflection, transmission coefficient, breast cancer, imaging, back propagation, forward propagation.

ENGINEERING JOURNAL Volume 21 Issue 2
Received 29 July 2016
Accepted 27 September 2016
Published 31 March 2017
Online at http://www.engj.org/
DOI:10.4186/ej.2017.21.2.237

DOI:10.4186/ej.2017.21.2.237

1. Introduction

Wireless communication has currently received huge amount of attention in biomedical engineering applications. Profound and probative research is underway to distinguish the behavior of biomedical communication and organic tissue channel models. The use of UWB transceivers is contemporary in this area for developing low cost, less invasive and high resolution communication systems.

Communication via human body is quite distinct compared to normal multipath wireless channel. For an organic medium, electromagnetic (EM) waves have to traverse several layers of tissues, having varying permittivity and conductivity values before reaching the receiver antenna. The bioelectric properties of these tissue layers (i.e. permittivity and conductivity) changes with frequency (dispersion) and time (relaxation constant). Therefore, obtaining an accurate channel model including the properties and effects of tissue medium, is very substantial in developing the communication system.

In particle physics and computational electromagnetic, scattering problem is perceived in two ways; direct scattering and inverse scattering [1]. Direct scattering problem determines the distribution of scattered radiation based on the characteristics of the scatterer. The inverse scattering problem determines the characteristics of an object (e.g., its shape, size, constitution) from receiving the signal scattered by the object. Most of the research work for breast cancer detection is focused in finding solutions to scattering problems for determining normal and tumor containing tissues [1-4]. Besides of the vast research works aiming to differentiate between healthy and tumorous breast tissues in excised samples using the pronounced differences in their scattering profiles. Now demand is to investigate the applicability of this technique for the recognition of breast tumor in the breast of a patient and the process is still confronting with many difficulties. Firstly, the data provided from the small-size excised breast tissue samples, normally in mm scale, is not sufficient to account for multiple scattering effects which affects the shape of scattered distribution in case of whole breast of normal dimension, is in average 100 to 120 mm. Secondly, it is not adequate to perform test measurements directly on patients because of the difficulties in correlating the measured profiles to a specific histopathology in breast tissue. Because of these problems, an alternative approach for performing research is on breast phantoms. At present, the available breast phantoms have only been used in mimicking the attenuation properties rather than producing an scattered profile distribution equivalent to breast tissue [5-9]. Another problem is gap between theoretical and experimental data values for making breast phantoms. In [10] a simple statistical procedure was developed to reduce the gap between the theoretical and experimental values for absolute permittivity of breast tissues.

In this paper, human breast phantom is considered for UWB communication system for early detection of breast tumor. The breast phantom data from [5, 8, 9] is used here. We have produced scattering profiles of this phantom by finding the S-parameters. S-parameters are reflection coefficient (S_{11}) and transmission coefficients (S_{12}). The scattering parameter values are then used to conceive the outcome of the breast medium. The results obtained will be used in future for the design of radio frequency RF filters, which can be employed at the front end in a UWB transceiver.

2. Multilayer Breast Model and Effective Permittivity

Wireless channel involving human body is quite different from a usual multipath channel. This is because, human body comprises of many layers of tissues and all have different dielectric properties contributing in the forward and scattered fields. Likewise, human breast is also divided into multiple tissue layers of skin, fat/adipose and glandular. In case in the presence of tumor cells, another layer is added up in this structure. Porter, et al. [5] developed practical heterogeneous phantoms by considering individual homogeneous phantoms for fat, skin, gland and tumor initially. Relative permittivity and conductivity for each phantom were measured at UWB microwave frequencies of 1 to 6 GHz. They also described a methodology to experimentally merge four phantoms into a single hemispherical heterogeneous breast phantom. The different layers of breast tissues with their relative permittivity and conductivity are shown in Tables 1 and 2 [6] respectively.

Table 1. Relative permittivity values for normal breast [5].

Frequency (GHz)	Relative Permittivity Values For:			
	Skin (F/m)	Fat/Adipose (F/m)	Gland (F/m)	Tumor (F/m)
1.0	40	15	35	59
1.5	39	14.5	34	57
2.0	38	14.2	33	56
2.5	37	14.0	32	55
3.0	36	13.8	31.8	54
3.5	35	13.5	31	53
4.0	34	13.2	30	52
4.5	33	13.0	29	50
5.0	32	12.5	28.5	47
5.5	31	12.0	28	46
6.0	30	11.0	27	45

Table 2. Conductivity values for normal breast [5].

Frequency (GHz)	Conductivity Values For:			
	Skin (S/m)	Fat/Adipose (S/m)	Gland (S/m)	Tumor (S/m)
1.0	0.5	0.5	0.2	0.5
1.5	0.6	0.1	0.5	0.7
2.0	0.8	0.2	0.8	1.2
2.5	1.5	0.3	1.0	2.0
3.0	1.8	0.4	1.5	2.2
3.5	2.3	0.5	2.0	2.8
4.0	2.5	0.6	2.2	3.5
4.5	3.2	0.7	2.4	4.2
5.0	3.8	1.0	2.8	5.1
5.5	4.2	1.2	3.2	5.5
6.0	4.8	1.3	3.8	6.2

Perez [14] in his Ph.D. dissertation (2012) explained the effective channel theory along with the effective permittivity of multilayer materials using Weiner absolute bounds [15]. He illustrated two cases. In the first case, incident wave is normal to the interfaces between layers and it was shown that the effective permittivity is equal to the sum of normalized weighted average function of the reciprocal of the permittivity values of individual layers. In the second case incident waves were parallel to the multiple layers and it was shown that the effective permittivity is sum of normalized weighted average function of the permittivity values of individual layers. In both cases, to any direction of incidence, direction of electric field vector, $\widehat{\mathrm{E}} - \mathrm{field}$, is always normal to the direction of propagation of wave incidence. These cases are explained in the following subsections.

A. Mathematical Description

The two cases can be correspondingly related to the series and parallel capacitors models (for two-layers) with known volume fractions. For parallel capacitor model, we have

$$\varepsilon_{\mathrm{eff}} = \xi_1 \varepsilon_1 + \xi_2 \varepsilon_2 \tag{1}$$

and for the series capacitor model,

$$\varepsilon_{eff}{}^{-1} = \xi_1 \varepsilon_1{}^{-1} + \xi_2 \varepsilon_2{}^{-1} \quad (2)$$

where ξ_1 and ξ_2 are the volume fractions of the constituent layers and ε_1 and ε_2 are the permittivity values of each layer. The constraint equation in this model is

$$\xi_1 + \xi_2 = 1 \quad (3)$$

Equation (3) implies that all the components' volume fractions sum the entire volume of the medium equal to unity.

B. Pictorial Representation

The example parallel and series plate capacitors models are shown in Fig. 1 in a transversal section with thickness t_1 and t_2 for the corresponding layers. Arrow shows direction of propagation of electric field.

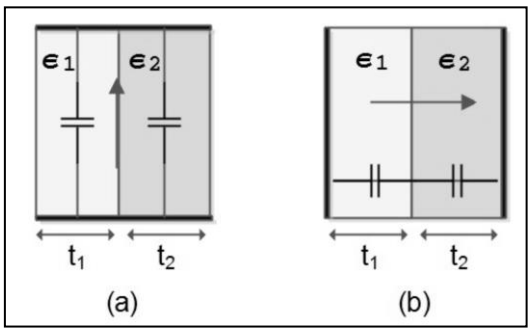

Fig. 1. Example (a) Parallel and (b) Series capacitor models to find effective permittivity [14].

It was found in [14] that if the interaction of electric field with the material interface is completely parallel, then Eq. (1) and Fig. 1(a) is the representation of it. However, if the interaction of electric field with the material interface is completely normal, then Eq. (2) and Fig. 1(b) is the representation.

Making use of these useful results, we take electric field being parallel to the interface of multi-layer breast. Therefore, Eq. (1) and Fig. 1(a) will be the desired model for finding effective permittivity.

3. Analytical Model for Scattering Parameters

Using Eq. (1) to (3), we can now easily find the effective permittivity for any multilayer medium. This simplifies the complex problem instead of solving each layer individually but taking it as a whole and finding the desired S- parameters from permittivity values.

Here we have assumed that incident signal is a plane wave (in the far field of the transmitting antenna) and it is normal to the dielectric surface. That is electric field ($\widehat{E}$) vector is parallel to the interface.

A. Calculation of Effective Permittivity

The complex permittivity is defined in [10] as

$$\varepsilon^* = \varepsilon' - j\varepsilon'' \quad (4)$$

where ε^* is the complex permittivity, the relative permittivity ε' is the real part of complex permittivity, and dielectric loss factor ε'' is the imaginary part of complex permittivity.

The conductivity, σ and dielectric loss factor, ε'' are related as [10]

$$\varepsilon'' = \frac{\sigma}{2\pi f \varepsilon_o} \quad (5)$$

Here, f is the frequency of communication, and ε_o is the permittivity for vacuum.

In the breast, skin covers 20%, adipose tissue covers 50% of the total breast and the rest 30% is glandular portion [16-17]. If we ad third layer of tuor in it then the latter normally covers 0.4% of the glandular part. Therefore, as calculated, the normalized volume fractions are $\xi_1 = 0.2, \xi_2 = 0.5, \xi_3 = 0.26$ and $\xi_4 = 0.04$ for skin, adipose, glandular and tumor respectively. Let $\varepsilon_1, \varepsilon_2, \varepsilon_3$ and ε_4 are the complex permittivity values of skin, fat, gland and tumor respectively then, using these values from Tables 1 and 2, to Eq. (1) and to (5), we get the complex effective permittivity for the heterogeneous breast with and without tumor as shown in Table 3 and 4, respectively. From the results in Table 3 and 4, the effective conductivity for the combined layers for normal and tumor containing breast is calculated using Eq. (5) and shown in Tables 5 and 6, respectively.

Table 3. Effective complex permittivity for heterogeneous normal breast.

Frequency (GHz)	Effective Complex Permittivity Values (F/m)
1.0	25.9650-j0.0057
1.5	25.2160-j0.0067
2.0	24.5670-j0.0139
2.5	23.9680-j0.0260
3.0	23.6082-j0.0421
3.5	23.0190-j0.0637
4.0	22.3700-j0.0811
4.5	21.7710-j0.1069
5.0	21.1715-j0.1458
5.5	20.6720-j0.1833
6.0	19.5730-j0.2292

Table 4. Effective complex permittivity for tumor containing breast.

Frequency (GHz)	Combined Effective Conductivity Values (S/m)
1.0	0.3174×10^{-3}
1.5	0.55909×10^{-3}
2.0	0.0015
2.5	0.0036
3.0	0.0070
3.5	0.0124
4.0	0.0180
4.5	0.0268
5.0	0.0406
5.5	0.0561
6.0	0.0765

Table 5. Effective conductivity for heterogeneous normal breast.

Frequency (GHz)	Effective Complex Permittivity Values (F/m)
1.0	28.3250-j0.0060
1.5	27.4960-j0.0072
2.0	26.8070-j0.0152
2.5	26.1680-j0.0288
3.0	25.7682-j0.0457
3.5	25.1390-j0.0691
4.0	24.4500-j0.0889
4.5	23.7710-j0.1174

Frequency (GHz)	Effective Complex Permittivity Values (F/m)
5.0	23.0515-j0.1600
5.5	22.4120-j0.2002
6.0	21.3730-j0.2499

Table 6. Effective conductivity for heterogeneous tumor containing breast.

Frequency (GHz)	Combined Effective Conductivity Values (S/m)
1.0	0.33379×10^{-3}
1.5	0.60082×10^{-3}
2.0	0.0017
2.5	0.0040
3.0	0.0076
3.5	0.0135
4.0	0.0198
4.5	0.0294
5.0	0.0445
5.5	0.0613
6.0	0.0834

B. Calculation and Simulation of Reflection and Transmission Coefficients

Following the instance of [18] analytical expressions of reflection coefficient, S_{11} and transmission coefficient S_{12} are

$$S_{11} = \frac{(k_0)^2-(k_1)^2}{(k_0+k_1)^2 e^{j4t(k_1)}-(k_0-k_1)^2} e^{j2tk_0} e^{(j4tk_1-1)} \tag{6}$$

$$S_{12} = \frac{k_0 k_1}{(k_0+k_1)^2 e^{j4t(k_1)}-(k_0-k_1)^2} 4e^{j2t(k_0+k_1)} \tag{7}$$

where

$$k_0 = \left(\frac{\omega}{c_0}\right) \tag{8}$$

and

$$k_1 = \sqrt{\varepsilon' \left(\frac{\omega}{c_0}\right)^2 - j\omega\mu_0\sigma} \tag{9}$$

with c_0 is the speed of electromagnetic waves in vacuum;
ω is the operating frequency of communication;
ε' is the real part of the effective permittivity;
t is the total thickness of the combined layers.

Derivations of Eq. (6) and (7) are provided in the Appendix for better understanding. Using Eq. (6) and (7), analytical values of the reflection and transmission coefficients can easily be obtained for the human breast model presented in Tables 3 and 4. The obtained numerical results are shown in Figs. 2 and 3 for UWB frequency band of 1 to 6 GHz. In these simulations following observations can be made readily:

1) The simulations are made from 1 to 6 GHz because of the availability of data from [5] for these frequency ranges only.
2) Reflection and transmission coefficients are exactly 180^o phase shifted at any frequency.
3) The trend of reflection and transmission coefficients are not constants but vary as the frequency varies. This is the process of dispersion.
4) The variations are directly related to variations in permittivity values as indicated by Eq. (6) and (7).
5) It is also seen that the trends are highly nonlinear. This is because the breast channel is a non-linear channel.
6) The consideration of operating frequency is very important. The behavior at one frequency is not similar as that of the other frequency.

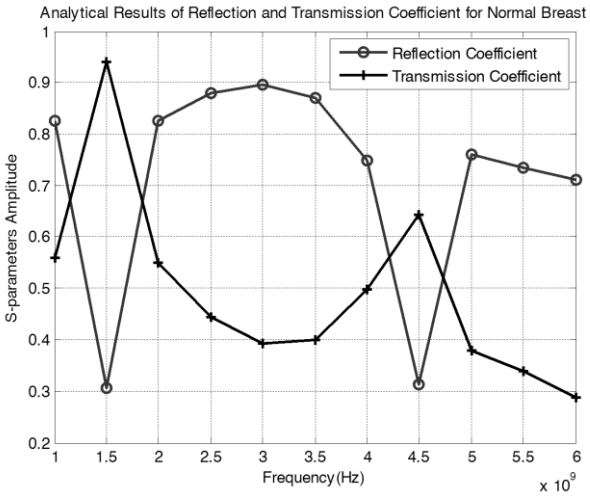

Fig. 2. Trends in reflection and transmission coefficients for normal breast.

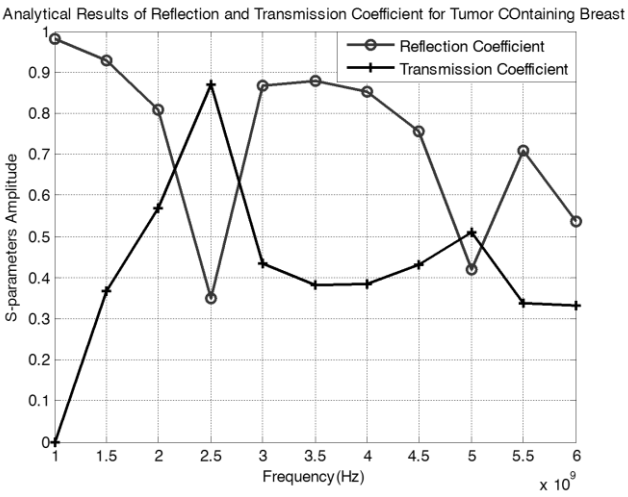

Fig. 3. Trends in reflection and transmission coefficients for tumor containing breast.

4. Conceiving Channel Impulse Response of Human Breast

Determination of reflection and transmission coefficients is useful in determining output behavior of the channel. To observe the channel behavior, we simulated the transmission of a Gaussian pulse (as planar wave) through the breast model.

The considered zero derivative Gaussian can be formulated as

$$E_0(t) = -e^{-\left(\frac{t-t_0}{\varsigma}\right)^2} \tag{10}$$

Here t_0 is the offset value of time (constant) and ς is the spreading factor (also constant).

UWB antennas are characterized to transmit next higher order derivative of the incident signal into the channel [20-22]. Therefore, in an actual system if this pulse is input to an antenna then its 1st derivative will be forwarded in to the channel. We used Matlab function gmonopuls ( ) for UWB center frequency of 4.5GHz with $\varsigma = 2$ and $t_0 = 0\ s$ to generate the first order derivative of Eq. (10) , as shown in Fig. 4.

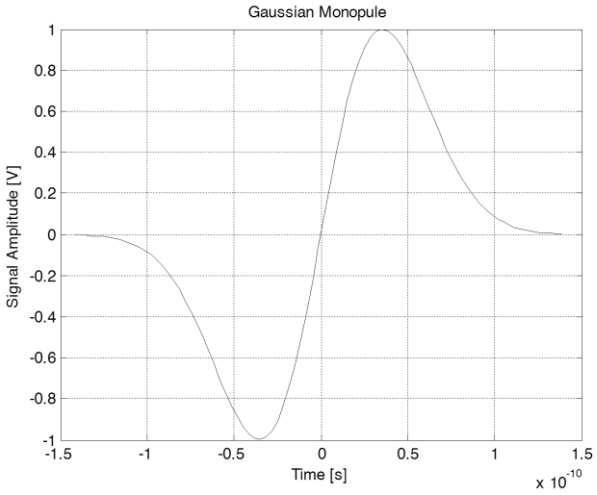

Fig. 4. First derivative Gaussian pulse generated in time domain for 4.5 GHz UWB center frequency.

The pulse in Fig. 4, is transmitted through the human breast to generate the reflected and transmitted waves. If $G(f)$ is the gain of the breast channel, $X(f)$ is the frequency domain representation of the time domain input signal $x(t)$ then output $Y(f)$ is the frequency domain representation of time domain output signal $y(t)$, and the later can be found as follows:

$$Y(f) = G(f)X(f) \tag{11}$$

Its time representative

$$y(t) = \mathcal{F}^{-1}(Y(f)) \tag{12}$$

Here, $\mathcal{F}^{-1}$ is the inverse Fourier transformation.

This is simulated for two ends of frequencies in the UWB band. One is lower with center frequency of the transmitted pulse to be equal to 2 GHz. Second simulations were carried out for higher end of UWB frequency set at 4.5 GHz.

4.1. Results of 1st Derivative Gaussian Pulse for Lower End of UWB

We simulated the breast channel, for backward and forward propagation gains in Figs. 5 and 6. The channel gains for backward propagation obtained from reflection coefficients at 2 GHz UWB center frequency are 0.8246 and 0.8098 for normal and tumorous breast respectively. Similarly, the channel gains for forward propagation obtained from transmission coefficient at same frequency are 0.5496 and 0.5691 for normal and tumorous breast respectively. The output (or received) signal y(t) is shown in Figs 5 and 6 for normal and tumorous breast respectively.

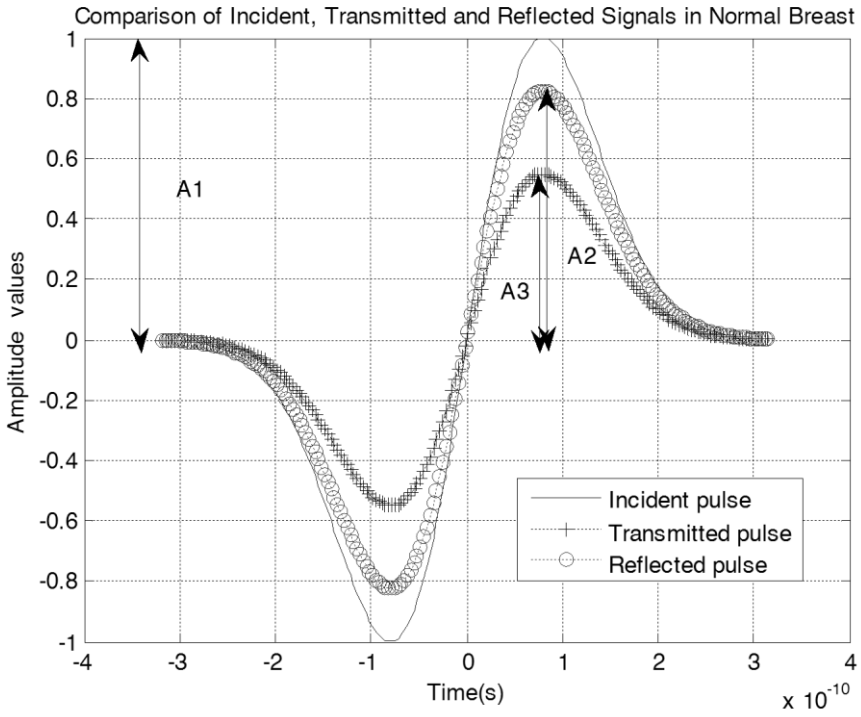

Fig. 5. Comparison of incident, reflected and transmitted pulse for normal breast at 2.0 GHZ UWB center frequency.

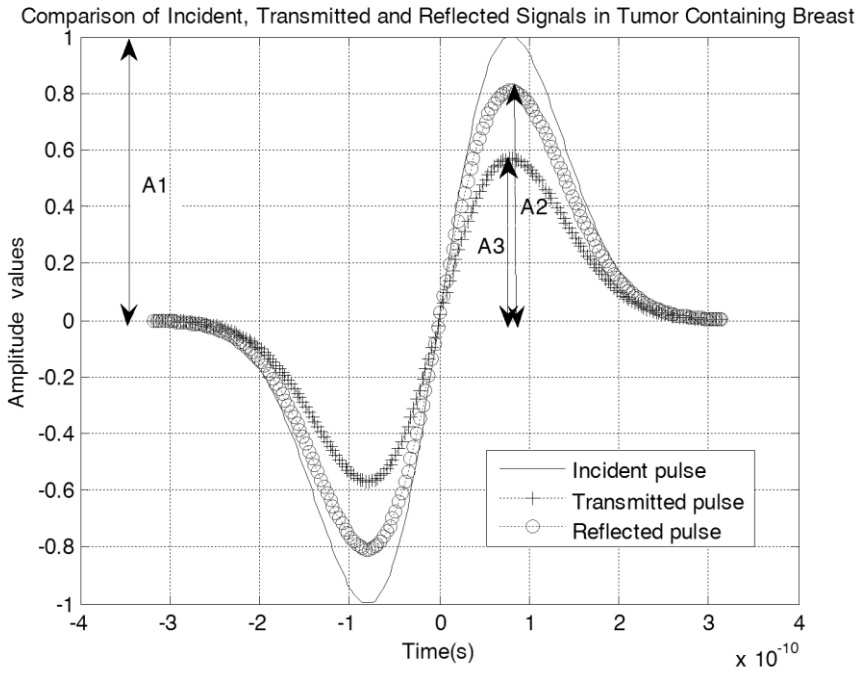

Fig. 6. Comparison of incident, reflected and transmitted pulse for tumor containing breast at 2.0 GHZ UWB center frequency.

4.2. Results of 1st Derivative Gaussian Pulse for Upper End of UWB

We further simulated the breast channel, for backward and forward propagation gains in Figs 7 and 8. The channel gains for backward propagation obtained from reflection coefficients at 4.5 GHz UWB center

frequency are 0.3127 and 0.7558 for normal and tumorous breast respectively. Similarly, the channel gains for forward propagation obtained from transmission coefficient at same frequency are 0.6426 and 0.4312 for normal and tumorous breast respectively. The output (or received) signal y(t) is shown in Figs 7 and 8 for normal and tumorous breast respectively.

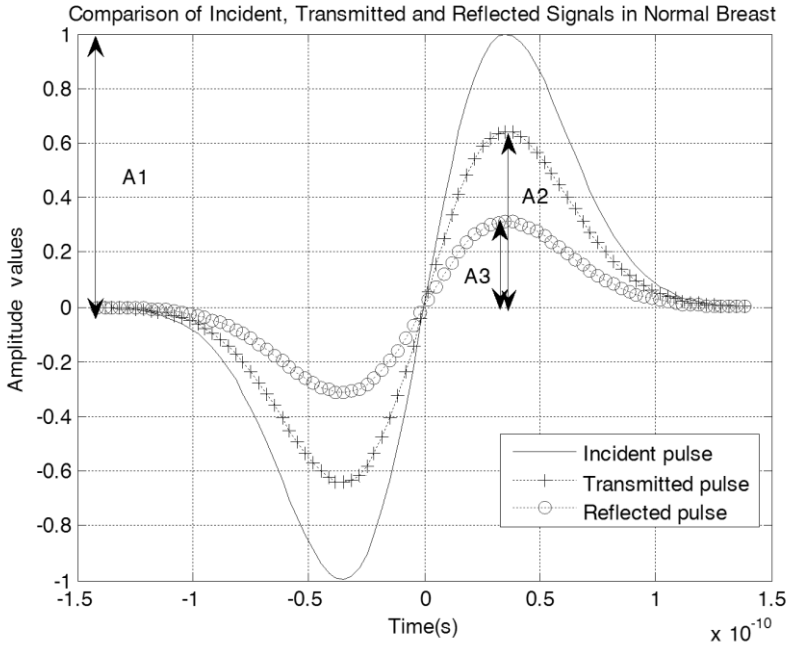

Fig. 7. Comparison of incident, reflected and transmitted pulse for normal breast at 4.5 GHZ UWB center frequency.

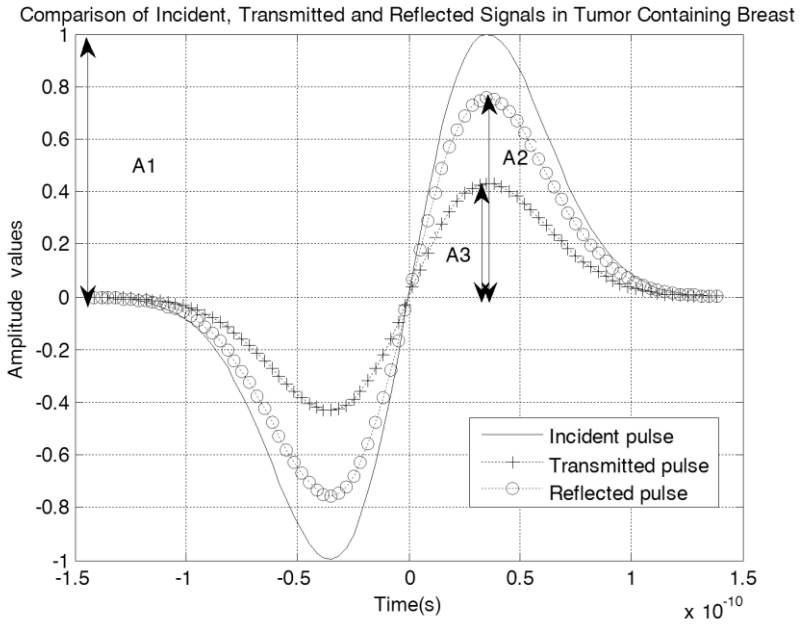

Fig. 8. Comparison of incident, reflected and transmitted pulse for tumor containing breast at 4.5 GHZ UWB center frequency.

It is observable from Figs 5 to 6 that however transmitted pulse from the antenna is always lower in amplitude as compared to the reflected signal in a normal breast and for a tumor containing breast. This is

observable from the amplitude markers A1, A2, and A3. Their corresponding amplitude values are directly interpretable from Figs. 5 and 6.

It is observable from Figs 7 to 8 that however transmitted pulse from the antenna is higher in amplitude as compared to the reflected signal in a normal breast but it is reverse for a tumor containing breast i.e. reflected signal is higher in amplitude in this case. This is observable from the amplitude markers A1, A2, A3 and B1, B2, B3 in Figs 5 to 7, respectively. Their corresponding amplitude values are directly interpretable from Figs. 7 and 8.

The percentage difference between two quantities is defined as the absolute value of the difference between the two scalars, divided by the mean of those two scalars, multiplied by 100%.

$$\text{percent difference} = \frac{|\text{difference of values}|}{\text{average of values}} \tag{13}$$

In the case of tumor containing breast, at 2.0 GHz (Fig. 6), the amplitude of reflected pulse is approximately $A_3 = 0.81$ units and amplitude of transmitted signal is approximately $A_2 = 0.58$. Therefore Eq. (13) is

$$\text{percent difference} = \frac{|0.81 - 0.51|}{\frac{0.81 + 0.51}{2}} = 45.45\%$$

Hence, from the simulations shown in Fig. 6, reflected signal is approximately 45.45 % higher in amplitude compared to the transmitted signal.

In the case of tumor containing breast, at 4.5 GHz (Fig. 8), the amplitude of reflected pulse is approximately $A_3 = 0.79$ units and amplitude of transmitted signal is approximately $A_2 = 0.41$. Therefore, Eq. (13) is

$$\text{percent difference} = \frac{|0.79 - 0.41|}{\frac{0.79 + 0.41}{2}} = 63.33\%$$

Hence, from the simulations shown in Fig. 8, reflected signal is approximately 63.3 % higher in amplitude compared to the transmitted signal. The amplitude of reflected and transmitted signals are directly related to the gain, i.e. S_{11} and S_{12}, values obtained from the curves in Figs. 2 and 3. It can be seen in these Figs that these S_{11} and S_{12} values show dispersive behavior with respect to changing frequency. Therefore, by obtaining the characteristic curves of S_{11} and S_{12}, we can easily determine to select reflected/scattered or transmitted signal in the design of the transceiver system.

5. Conclusion

In this paper work has been carried out to successfully determine effective dielectric properties and scattering parameters characteristics for lower end of UWB frequency band using analytical formulations of heterogeneous human breast. It is found that due to dispersive nature of breast, reflection and transmission coefficients also show dispersion with frequency change. For normal breast reflected/scattered signal was low but in the case of tumor containing breast reflected signal was remarkably high as compared to the transmitted signal. Hence for the early detection of breast cancer, it is more advantageous to design transceivers which work on the principal of back-propagation (capturing reflected signals). To design the transceiver for whole UWB range the characteristic reflection and transmission coefficient curves that we have obtained here, can be used as a guideline to determine the use of reflected or forward propagated signals for the communication link through the breast at any center frequency in the UWB band.

DOI:10.4186/ej.2017.21.2.237

Appendix

In order to derive the analytical expressions for transmission and reflection coefficients, we consider the scenario shown in Fig A-1. This is divided in three regions. They are '0', '1' and '0' for the incident, channel and forward transmitted regions respectively. Here, '0' indicates the air region and '1' indicates the body tissue medium. These regions are separated by boundaries named A and B. Region 0 is the region where incident signal comes, and incident signal $\psi_{inc} = 1$. It is then forward propagated and reflected as shown in the Fig A-1 with respect to the reflection coefficients and transmission coefficients defined at the boundaries A and B. Some important definitions used in this derivation are:

r_{01} = reflection coefficient at interface A between regions 0 & 1;
r_{10} = reflection coefficient at interface B between regions 1 & 0;
t_{01} = transmission coefficient at interface A between regions 0 & 1;
t_{10} = transmission coefficient at interface B between regions 1 & 0;
k_1 = propagation constant for region 1 with zero attenuation;
k_0 = propagation constant for region 0 with zero attenuation;
a = thickness of channel / region 1.

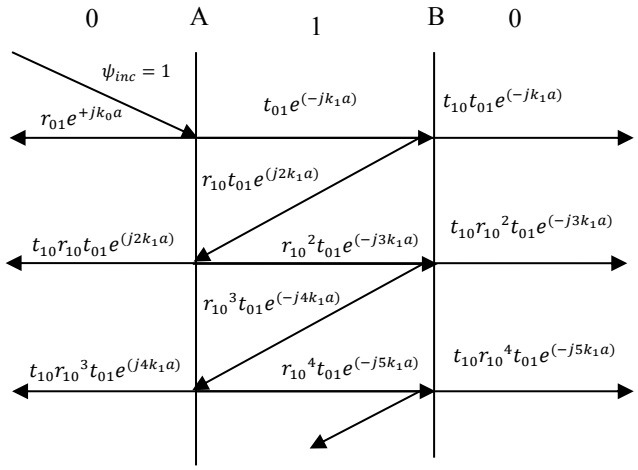

Fig. A-1. Wave functions resulting from the incident ψ signal by successive transmission and reflection.

Total transmitted signal ψ_{trans} comes out can be defined as,

$$\psi_{trans} = t_{10}t_{01}e^{(-jk_1a)} + t_{10}r_{10}{}^2t_{01}e^{(-j3k_1a)} + t_{10}r_{10}{}^4t_{01}e^{(-j5k_1a)} + \cdots \quad (A.1)$$

Simplifying Eq. (A.1), we have

$$\psi_{trans} = t_{10}t_{01}e^{(-jk_1a)}\left[1 + r_{10}{}^2e^{(-j2k_1a)} + r_{10}{}^4e^{(-j2k_1a)} + \cdots\right] \quad (A.2)$$

By applying summation on the geometric series inside the braces in Eq. (A.2) and using the definition, that $r_{10} = -r_{01}$, we have

$$\psi_{trans} = \frac{t_{10}t_{01}e^{(-jk_1a)}}{[1-r_{01}{}^2e^{(-j2k_1a)}]} \quad (A.3)$$

We know that

$$k_0 = \left(\frac{\omega}{c_0}\right) \quad (A.4)$$

$$k_1 = \sqrt{\varepsilon' \left(\frac{\omega}{c_0}\right)^2 - j\omega\mu_0\sigma} \tag{A.5}$$

and refractive index n and propagation constants k are related by

$$n = \frac{c}{\omega}k \tag{A.6}$$

where c is the speed of light or EM waves in the vacuum, and ω is angular frequency of EM wave and k is the propagation constant for any medium.

Propagation constant and reflection coefficient at the boundaries are defined by

$$\left.\begin{aligned} t_{10} = \frac{2n_1}{(n_1+n_0)}, t_{01} = \frac{2n_0}{(n_0+n_1)}, r_{01} = \frac{(n_0-n_1)}{(n_0+n_1)} \end{aligned}\right\} \tag{A.7}$$

Taking $\frac{c}{\omega}$ as constant at a particular frequency and using Eq. (A.6) in Eq. (A.7), we have

$$t_{10} = \frac{2\frac{c}{\omega}k_1}{(\frac{c}{\omega}k_{1_1} + \frac{c}{\omega}k_0)}, t_{01} = \frac{2\frac{c}{\omega}k_0}{(\frac{c}{\omega}k_{1_1} + \frac{c}{\omega}k_0)}, r_{01} = \frac{(\frac{c}{\omega}k_0 - \frac{c}{\omega}k_1)}{(\frac{c}{\omega}k_0 + \frac{c}{\omega}k_1)}$$

which after simplification becomes

$$\left.\begin{aligned} t_{10} = \frac{2k_1}{(k_1+k_0)}, t_{01} = \frac{2k_0}{(k_0+k_1)}, r_{01} = \frac{(k_0-k_1)}{(k_0+k_1)} \end{aligned}\right\} \tag{A.8}$$

Putting the values of t_{10}, t_{01} and r_{01} in Eq. (A.3) we have after simplification as

$$\psi_{trans} = \frac{4k_1k_0e^{(-jk_1a)}}{e^{(-j2k_1a)}[e^{(j2k_1a)}(k_0+k_1)^2 - (k_0-k_1)^2]}$$

or

$$\psi_{trans} = \frac{4k_1k_0e^{(jk_1a)}}{[e^{(j2k_1a)}(k_0+k_1)^2-(k_0-k_1)^2]} \tag{A.9}$$

Since the incident signal $\psi_{inc} = 1$, then Eq. (A.9) is the transmission coefficient as, transmission coefficient, T, is

$$T = \frac{\psi_{trans}}{\psi_{inc}} \tag{A.10}$$

In general, for any other incident signal with phase term defined with $\psi_{inc} = e^{(-jk_0a)}$, then transmission coefficient of Eq. (A.9) becomes

$$T = \frac{4k_1k_0e^{(jk_1a)}e^{(jk_0a)}}{[e^{(j2k_1a)}(k_0+k_1)^2-(k_0-k_1)^2]} \tag{A.11}$$

If the medium in region 1 is symmetric then the thickness of this region can be considered as $a = 2t$, then Eq. (A.11) becomes,

$$T = \frac{4k_1k_0e^{j2t(k_1+k_0)}}{[e^{(j4k_1t)}(k_0+k_1)^2-(k_0-k_1)^2]} \tag{A.12}$$

In a similar manner like written as in Eq. (A.13) and Fig. A-1, the received signal, ψ_{rec} can be followed by the final version as in Eq. (A.14).

$$\psi_{rec} = \frac{r_{01} - r_{01} e^{(j2k_1 a)}}{[1 - r_{01}{}^2 e^{(j2k_1 a)}]} \tag{A.13}$$

$$\psi_{rec} = \frac{(k_0{}^2 - k_1{}^2)(e^{j2k_1 a} - 1)}{[e^{(j2k_1 a)}(k_0 + k_1)^2 - (k_0 - k_1)^2]} \tag{A.14}$$

Since the incident signal $\psi_{inc} = 1$, then Eq. (A.14) is the reflection coefficient, because the reflection coefficient, Γ, is

$$\Gamma = \frac{\psi_{rec}}{\psi_{inc}} \tag{A.15}$$

For any other incident signal with phase $\psi_{inc} = e^{(-jk_0 a)}$, the reflection coefficient in Eq. (A.14) becomes

$$\Gamma = \frac{(k_0{}^2 - k_1{}^2)(e^{jk_0 a})(e^{j2k_1 a} - 1)}{[e^{(j2k_1 a)}(k_0 + k_1)^2 - (k_0 - k_1)^2]} \tag{A.16}$$

Followed by for a symmetric medium Eq. (A.16) becomes

$$\Gamma = \frac{(k_0{}^2 - k_1{}^2)(e^{j2k_0 t})(e^{j4k_1 t} - 1)}{[e^{(j4k_1 t)}(k_0 + k_1)^2 - (k_0 - k_1)^2]} \tag{A.17}$$

References

[1] G. L. Gragnani and M. Diaz Mendez, "Improved electromagnetic inverse scattering procedure using non-radiating sources and scattering support reconstruction," *Microwaves, Antennas & Propagation*, vol. 5, no. 15, pp. 1822–1829, Dec. 9, 2011.

[2] T. P. Ketterl, G. E. Arrobo, A. Sahin, T. J. Tillman, H. Arslan, and R. D. Gitlin, "In vivo wireless communication channels," in *Wireless and Microwave Technology Conference (WAMICON), 2012 IEEE 13th Annual*, Apr. 15-17, 2012, pp. 1–3.

[3] M. A. Ali and M. Moghaddam, "3D nonlinear super-resolution microwave inversion technique using time-domain data," *Antennas and Propagation, IEEE Transactions on*, vol. 58, no. 7, pp. 2327–2336, Jul. 2010.

[4] J. E. Johnson, T. Takenaka, K. A. H. Ping, S. Honda, and T. Tanaka, "Advances in the 3-D forward–backward time-stepping (FBTS) inverse scattering technique for breast cancer detection," *Biomedical Engineering, IEEE Transactions on*, vol. 56, no. 9, pp. 2232–2243, Sep. 2009.

[5] E. Porter, J. Fakhoury, R. Oprisor, M. Coates, and M. Popović, "Improved tissue phantoms for experimental validation of microwave breast cancer detection," in *Antennas and Propagation (EuCAP), 2010, Proceedings of the Fourth European Conference on*, Apr. 12-16, 2010, pp. 1-5.

[6] J. C. Y. Lai, C. B. Soh, E Gunawan, and K. S. Low, "Homogeneous and heterogeneous breast phantoms for ultra-wideband microwave imaging applications," *Progress In Electromagnetics Research, PIER*, vol. 100, pp. 397-415, 2010

[7] S. Alshehri, S. Khatun, and Z. Awang, "Homogeneous and heterogeneous breast phantoms for UWB imaging," in *ISABEL'11, Proceedings of the 4th International Symposium on Applied Sciences in Biomedical and Communication Technlogies*, Barcelona, Spain, ACM, 2011

[8] E. Porter, A. Santorelli, D. Coulibaly, M. Coates, and M. Popovic, "Time-domain microwave breast screening system: Testing with advanced realistic breast phantoms," in *Antennas and Propagation (EUCAP), 2012 6th European Conference on*, Mar. 26–30, 2012, pp. 1766–1769.

[9] M. S. Hathal, T. F. A. Zanoon, M. F. Ain, and M. Z. Abdullah, "Experimental ultra wide band imaging using heterogeneously dense breast phantom for early cancer detection," in *Imaging Systems and Techniques (IST), 2012 IEEE International Conference on*, July 16–17, 2012, pp. 130–135.

[10] E. Ikram, K. Sabira, K. Jahid Reza, M. Mijanur, and F. Moslemuddin, (2013). Improved debye model for experimental approximation of human breast tissue properties at 6 GHz ultra-wideband centre frequency.

[11] C.-H. Kuo and M. Moghaddam, "Electromagnetic scattering from a buried cylinder in layered media with rough interfaces," in *Antennas and Propagation Society International Symposium 2006, IEEE*, July 9–14, 2006, pp. 653–656.
[12] M. B. Protsenko and I. Y. Rozhnovskaya, "Description of radio channel with random polarization structure in terms of matrix of S-parameters," in *Proc. Mathematical Methods in Electromagnetic Theory (MMET), 2012 International Conference on*, Aug. 28–30, 2012, pp. 569–572.
[13] E. A. Gonzalez, I. Petras, L. Dorcak, and J. Terpak, "On the mathematical properties of generalized fractional-order two-port networks using hybrid parameters," in *Proc. Carpathian Control Conference (ICCC), 2013, 14th International*, May 26–29, 2013, pp. 88–93.
[14] M. D. Cesaretti Pérez, "General effective medium model for the complex permittivity extraction with an open-ended coaxial probe in presence of a multilayer material under test," Ph.D. dissertation, University of Bologna, Italy, 2012.
[15] G. W. Milton, "Bounds on the complex permittivity of a two-component composite material," *Journal of Applied Physics*, vol. 52, no. 8, pp. 5286-5293, 1981.
[16] Computerized Imaging Reference Systems, Inc. *Tissue Equivalent Phantoms for Mammography, Models 010 & 011*, 2011
[17] S. Wong, A. Kaur, M. Back, K. M. Lee, S. Baggarley, and J. J. Lu, "An ultrasonographic evaluation of skin thickness in breast cancer patients after postmastectomy radiation therapy," *Radiation Oncology*, vol. 6, no. 9, pp. 1-10, 2011.
[18] B. Anders, T. Rylander, and P. Ingelström, *Computational Electromagnetics*. New York: Springer, 2005, vol. 51, pp. 235-236.
[19] I. E. Khuda, M. G. Tahir, and K. Raza, "Novel channel impulse response equations of normal and malignant skin at high frequency MM-wave band," *Sci. Int.*, vol. 28, no. 2, pp. 885-889, 2016.
[20] J. R. Andrews, "UWB signal sources, antennas and propagation," in *Proc. Wireless Communication Technology, 2003. IEEE Topical Conference on*, Oct. 15–17, 2003, pp. 439–440.
[21] A. H. Mohammadian, A. Rajkotia, and S. S. Soliman, "Characterization of UWB transmit-receive antenna system," in *Proc. Ultra Wideband Systems and Technologies, 2003 IEEE Conference on*, Nov. 16–19, 2003, pp. 157–161.
[22] D. Ghosh, A. De, M. C. Taylor, T. K. Sarkar, M. C. Wicks, and E. L. Mokole, "Transmission and reception by ultra-wideband (UWB) antennas," *Antennas and Propagation Magazine, IEEE*, vol. 48, no. 5, pp. 67–99, Oct. 2006. [Online]. Available: http://www.phy.ilstu.edu/slh/percent%20difference%20error.pdf